Numerical studies of free exciton and trion wave functions in high magnetic fields

Arkadiusz Wójs
Institute of Physics, Wroclaw University of Technology, Wybrzeże Wyspiańskiego 27, 50-370 Wroclaw, Poland
(Received 22 April 2007; revised manuscript received 3 July 2007; published 28 August 2007)

Wave functions of excitons and negative and positive trions confined in GaAs quantum wells and subject to high magnetic fields are studied by exact numerical diagonalization in Haldane spherical geometry. Finite width of the quantum well and its asymmetry caused by one-sided doping are both fully taken into account by using self-consistent subband wave functions in the integration of Coulomb matrix elements and by inclusion of multiple electron and hole subbands and Landau levels in the configuration-interaction basis. The main results regard the interaction-induced mixing of electron and hole single-particle levels, normal charge density profiles, in-plane correlation functions, and optical oscillator strengths. These characteristics are calculated for the exciton and different trion states, in terms of their dependence on the quantum-well width, carrier concentration, and magnetic field.

DOI: 10.1103/PhysRevB.76.085344 PACS number(s): 71.35.Pq, 71.35.Ji, 71.10.Pm

I. INTRODUCTION

This paper follows immediately on our recent work[1] on trion binding energies in high magnetic fields. Trions[2–4] ($X^{\pm}=X+e$ or h) form in doped semiconductor nanostructures from neutral excitons ($X=e+h$) by the capture of another electron (e) or hole (h). The energy spectra of such three-body complexes in different systems contain one or more bound states distinguished by the relevant conserved spin and orbital quantum numbers. For example, in two dimensions and in high magnetic fields, one more of the following states may occur: "bright singlet,"[5–7] "dark triplet,"[8–10] "bright triplet,"[11,12] and "dark singlet,"[1] with the ground state depending on the particular parameters.[11–15] The fairly rich trion dynamics is a consequence of the competition of several energy and length scales, driven by the interplay of interactions, confinement, and electric and magnetic fields. On the other hand, the importance of trions in the context of optical properties of nanostructures arises from their being robust radiative quasiparticles, dominating the photoluminescence (PL) spectra through a wide range of experimental conditions.[16–21] This is quite remarkable in view of the fact that the trion's stability must naturally be undermined by the collisions with the surrounding free carriers, present necessarily for the trion formation.

The robustness of magnetotrions in two dimensions is attributed to the unique, Laughlin form of the e-X^{-} and h-X^{+} correlations[22] characteristic of the charged particles in a partially filled lowest Landau level (LL). By an effective spatial isolation of the trions from the surrounding carriers, Laughlin correlations prevent their strong perturbation by the high-energy e-X^{-} or h-X^{+} scattering.[11] Certainly, even in those so-called quantum Hall systems, when the carrier concentration grows too high (corresponding to the LL filling fraction ν approaching about one-third), the trions become too strongly coupled to the surrounding Laughlin liquid and can no longer be considered well-defined three-body quasiparticles. However, it was recently suggested[23,24] that in this regime, new radiative complexes called "quasiexcitons" form from trions through partial (fractional) screening of their charge by the liquid. Since the quasiexciton energy and recombination spectrum depend critically on the particular trion ground state in the given conditions (e.g., width of the quasi-two-dimensional layer, magnetic field, or electric field due to asymmetric doping), trion dynamics remains of interest far beyond the dilute regime of $\nu \ll 1$.

The binding energies of negative and positive magnetotrions in doped GaAs quantum wells were recently studied in Ref. 1. The present paper is an immediate continuation of that work, focusing on the exciton and trion wave functions instead of the energy spectra. We use the same model and numerical scheme and thus do not repeat here their details or justification. The slight improvement is the expansion of the trion configuration-interaction basis by adding the third quantum-well subband (in order to allow better description of the earlier suggested dynamical narrowing of the hole subband wave function). Compared to the earlier models, by exact diagonalization in the Hilbert space including multiple single-particle excitations in all three spatial dimensions, we fully take into account the above-mentioned crucial interplay of Coulomb interactions, strong quantum-well confinement, strong perpendicular magnetic field, and (in asymmetrically doped wells) significant electric field—all together defining the complexity of the trion dynamics in realistic experimental conditions.

For both excitons and trions, we study the efficiency of subband and LL mixing, electron and hole normal charge density profiles, in-plane correlation functions, and the oscillator strengths for optical transitions. These characteristics are analyzed in terms of their dependence on the relevant experimental parameters: quantum-well width w, carrier concentration ϱ, and magnetic field B. Only free excitons and trions are discussed, and the binding to ionized impurities will be addressed in a separate publication.

II. MODEL

The model used in the present calculation has been explained in detail in Ref. 1. In short, we first use planar geometry to solve the one-dimensional electron and hole Schrödinger-Poisson problems in a given quantum well. The subband wave functions are then used to calculate the three-

TABLE I. Binding energies Δ (in meV) of different negative and positive trion states (sb, bright singlet; td, dark triplet; tb, bright triplet; and sd, dark singlet) calculated on a sphere with monopole strength $2Q=20$ including five LLs and two or three quantum-well subbands ($s_{\max}=1$ or 2) for electrons and holes, in several different quantum-well systems labeled as A–F and defined by "w ϱ B" (in nm, 10^{11} cm^{-2}, and T, respectively). $\varrho>0$ means electron (hole) concentration for X^- (X^+), "—" means "unbound," and the values for $s_{\max}=2$ (in boldface) are new compared to Ref. 1.

System	$s_{\max}$	Δ^-_{sb}	Δ^-_{td}	Δ^-_{tb}	Δ^-_{sd}	Δ^+_{sb}	Δ^+_{td}	Δ^+_{tb}	Δ^+_{sd}
A	1	1.95	1.16	0.29	—	1.10	1.28	0.36	0.35
15 0 15	2	**2.09**	**1.16**	**0.29**	—	**1.14**	**1.28**	**0.36**	**0.32**
B	1	2.00	1.46	0.32	—	1.04	1.46	0.33	0.46
15 0 25	2	**2.22**	**1.49**	**0.34**	—	**1.11**	**1.46**	**0.32**	**0.42**
C	1	1.90	1.42	0.29	—	0.84	1.29	0.23	0.37
15 2 25	2	**2.12**	**1.50**	**0.36**	—	**0.95**	**1.33**	**0.28**	**0.37**
D	1	1.74	1.11	0.28	—	0.99	1.18	0.32	0.37
20 0 15	2	**1.96**	**1.14**	**0.30**	—	**1.04**	**1.16**	**0.31**	**0.33**
E	1	1.75	1.36	0.29	0.05	0.95	1.32	0.28	0.46
20 0 25	2	**2.07**	**1.43**	**0.34**	**0.01**	**1.04**	**1.30**	**0.27**	**0.39**
F	1	1.51	1.24	0.21	0.05	0.60	0.95	0.10	0.21
20 2 25	2	**1.72**	**1.30**	**0.27**	**0.04**	**0.68**	**0.94**	**0.13**	**0.17**

dimensional Coulomb matrix elements in Haldane spherical geometry.[26] Finally, the $e+h$, $2e+h$, and $2h+e$ Hamiltonians are diagonalized numerically in the full configuration-interaction basis using Lanczos algorithm with the simultaneous resolution of spin and angular momentum (method similar to that of Ref. 27).

The magnetic monopole strength of the Haldane sphere is chosen as $2Q=2\sqrt{Q}$. This sets the sphere radius $R=\sqrt{Q}\lambda$, where $\lambda=\sqrt{\hbar c/eB}$ is the magnetic length (the surface curvature effects at this finite radius were earlier found[1] insignificant). The bases are restricted to a number of lowest electron and hole quantum-well subbands and LLs ($s_e, s_h \leqslant s_{\max}$ and $n_e, n_h \leqslant n_{\max}$).

Compared to Ref. 1, we were able to include one more subband ($s_{\max}=2$) in a five LL calculation ($n_{\max}=4$) also for the trions. This boosts the dimension of the trion Hamiltonian to over 1.5×10^6 and the number N_H of its above-diagonal nonzero matrix elements to $\sim10^{10}$ (although in symmetric wells, this number is reduced by half due to the parity conservation). Since even with compression such big Hamiltonians take about 120 Gbytes of memory, the major problems we had to overcome were matrix storage and efficient matrix-vector multiplication.

III. RESULTS AND DISCUSSION

A. Binding energies

In Table I (in boldface), we list several trion binding energies Δ which improve over our earlier estimates[1] obtained for $s_{\max}=1$. (In Fig. 1, we also plot sample dependences of Δ on w and B.) Note that the improvement and thus also the uncertainty of the present best estimates are (by far and in each system we looked at) the largest for the negative bright singlet trion. The stronger sensitivity to the subband mixing in X^-_{sb} than in the other X^- states could be expected from the fact that the pair of electrons in X^-_{sb} largely occupies the same orbital and thus most strongly interacts with one another. However, the much weaker sensitivity found for all positive trions (including X^+_{sb}) is rather unexpected in view of their involving two holes (i.e., particles with a low intersubband excitation gap) instead of one. Explanation of this result will be postponed till Fig. 12; it is related to another curious prediction of Table I that Δ^+_{sb} seems always about twice smaller than Δ^-_{sb} in the same symmetric well. Summarizing Table I, we also find that (i) the most strongly bound trion is the X^-_{sb}; (ii) the X^-_{sd} is at most marginally bound, in contrast to X^+_{sd} (note, however, that the Coulomb binding of all singlet states must overcome the electron or hole Zeeman energy E_Z to ensure their stability and a possible signature in PL); (iii) compared to the singlets, the binding energies of both triplets

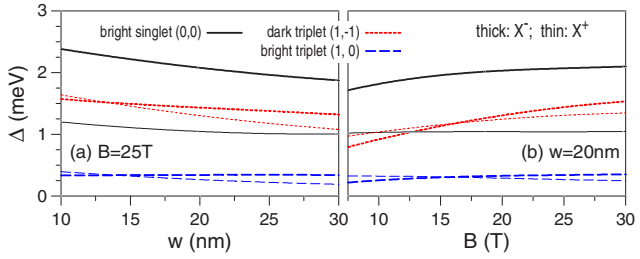

FIG. 1. (Color online) Binding energies Δ of different states of the negative and positive trions, labeled as $(S,\mathcal{M})$ by the pair electron-hole spin $S=0$ or 1 (singlet or triplet) and the relative angular momentum $\mathcal{M}$, drawn as a function of (a) well width w and (b) magnetic field B.

are far less sensitive to the trion's charge sign; (iv) of all binding energies, $\Delta_{td}^{\pm}$ show the strongest dependence on w and B; and (v) one-sided doping with donors affects Δ_{td}^{-} much less than it affects Δ_{sb}^{-}, but the reduction of both Δ_{sb}^{+} and Δ_{td}^{+} due to one-sided doping with acceptors is strong (and about equal).

Let us also try to establish the absolute trion ground state in each system listed in Table I. As mentioned above, since the competing states ($X_{sb}^{\pm}$ and $X_{td}^{\pm}$) differ by a spin flip, $\Delta_{td}^{\pm}$ must be compared with $\Delta_{sb}^{\pm}-E_Z$ to determine lower total energy. For the positive trions, the answer is simple: $\Delta_{td}^{+}>\Delta_{sb}^{+}$ and X_{td}^{+} is the ground state in all listed systems (regardless of the precise value of the hole E_Z). For the negative trions, $\Delta_{td}^{-}<\Delta_{sb}^{-}$, and the answer depends on electron E_Z. Fortunately, the width dependence of the effective electron Landé factor $g^*(w)$ is known quite accurately.[28] In particular, $g^*(20\ \text{nm})=-0.40$ and $g^*(15\ \text{nm})=-0.35$, yielding $\Delta_{sb}^{-}-E_Z=1.79$, 1.71, 1.61, 1.61, 1.49, and 1.14 meV in A, B, C, D, E, and F. Clearly, X_{sb}^{-} is the ground state in A, B, C, and D, X_{td}^{-} is the ground state in F, and the two states come close to the crossing in E. Importantly, confirmation of the X_{td}^{-} ground state in the narrower, doped well F supports the quasiexciton theory[23] of the PL discontinuity observed[24] in such a sample at $\nu=\frac{1}{3}$.

B. Failure of lowest Landau level and/or subband approximations

Let us begin the discussion of exciton and trion wave functions with the test of natural approximations consisting of the confinement of electrons and holes to their respective lowest LLs ($n=0$) and/or lowest quantum-well subbands ($s=0$). Obviously, the former could be anticipated to work better at very high magnetic fields (when the cyclotron gap $\hbar\omega_c$ becomes large compared to the Coulomb energy scale e^2/λ), while the latter might be justified in narrow wells (with a large intersubband gap $\mathcal{E}_1-\mathcal{E}_0$). However, the fact that the bright singlet trion remains bound even at the highest studied fields[29–31] demonstrates that the lowest LL limit is quite unrealistic (owing to the "hidden symmetry,"[32] the only two-dimensional (2D) trion bound in the lowest LL should be the dark triplet[9]). On the other hand, the efficiency of subband mixing in the exciton and different trions and their dependence on sample parameters have not been earlier analyzed in detail (although, admittedly, the lowest-subband approximation was questioned in sufficiently wide symmetric wells[13]).

To test the lowest LL and lowest-subband approximations, we have calculated projections of the accurate exciton and trion eigenstates Ψ onto the $s=0$, $n=0$, and $s=n=0$ subspaces. In Figs. 2 and 3, we plot results for the exciton whose energy spectrum was obtained from exact diagonalization in the e-h basis restricted to $s\leqslant 2$ and $m\leqslant 4$. In each frame, the thick solid black line gives the squared projection onto $s=n=0$, i.e., $\xi_{\text{LL,sub}}^2=|\hat{\mathcal{P}}_{s=0}\hat{\mathcal{P}}_{n=0}\Psi|^2$. For comparison, a pair of thinner lines, dotted blue and dashed red, represent $\xi_{\text{sub}}^2=|\hat{\mathcal{P}}_{s=0}\Psi|^2$ and $\xi_{\text{LL}}^2=|\hat{\mathcal{P}}_{n=0}\Psi|^2$, respectively. More precisely, we plot $1-\xi^2$ (a direct measure of the LL and/or subband mixing) rather than ξ^2 itself.

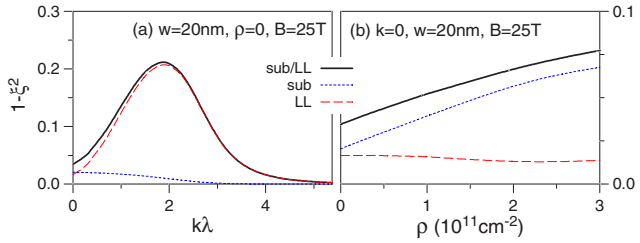

FIG. 2. (Color online) Efficiency of quantum-well subband (sub) and Landau level (LL) mixing in the exciton eigenstates. The ξ^2 denotes the squared projection onto the $s=0$ (sub), $n=0$ (LL), or $s=n=0$ (sub/LL) subspace, and $1-\xi^2$ is drawn as a function of the (a) excitonic wave vector k [λ is the magnetic length] or (b) electron sheet concentration ϱ.

Figure 2(a) shows, on the example of a symmetric $w=20$ nm well at $B=25$ T, the dependence on the excitonic wave vector k. In this particular system, subband mixing is not strong, and it gradually disappears with the increase of k as a result of the weakening e-h interaction. In contrast, the LL mixing is the strongest at intermediate wave vectors, with $1-\xi^2$ rising from 0.02 to 0.21 between $k\lambda=0$ and 2. The relatively weak LL mixing at small k is caused by the conservation of two in-plane orbital quantum numbers in the Coulomb scattering (on a sphere, length and projection of the pair angular momentum, L and L_z; on a plane, "relative" and total angular momenta,[33] $\mathcal{M}$ and M). As a result, the $k=0$ excitonic ground state does not couple to those configurations with e and h being in two different LLs, in particular, to the $n_e=0$ and $n_h=1$ subspaces, despite its low cyclotron excitation energy. This k-induced relaxation of the n-selection rule makes $1-\xi_{\text{LL}}^2(k)$ nonmonotonic, in contrast to $1-\xi_{\text{sub}}^2(k)$ for which the corresponding s-selection rule does not depend on k. A dynamical consequence of the enhanced LL mixing at intermediate values of k is flattening of the excitonic dispersion as small k (enhancement of the exciton "Coulomb mass") discussed earlier in Ref. 1.

A similar nonmonotonic dependence occurs for $1-\xi_{\text{sub}}^2(\varrho)$ shown in Fig. 2(b) for the $k=0$ excitonic ground state. Here, asymmetry of the quantum-well appearing at $\varrho>0$ (for one-sided doping) allows for parity mixing; in particular, excitations to the low-energy $s_e=0$ and $s_h=1$ subspace become available. On the other hand, too large ϱ results in too weak e-h interaction, thereby diminishing the subband-mixing effect. An obvious dynamical sign of the enhanced subband mixing at intermediate ϱ is a considerably

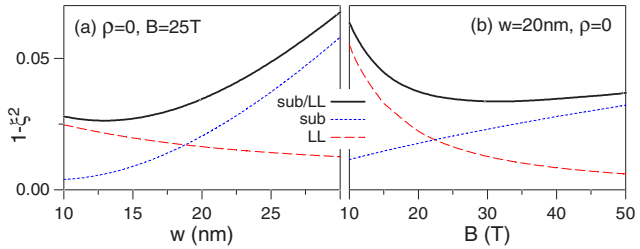

FIG. 3. (Color online) Same as Fig. 2 but with $1-\xi^2$ drawn as a function of the (a) well width w or (b) magnetic field B.

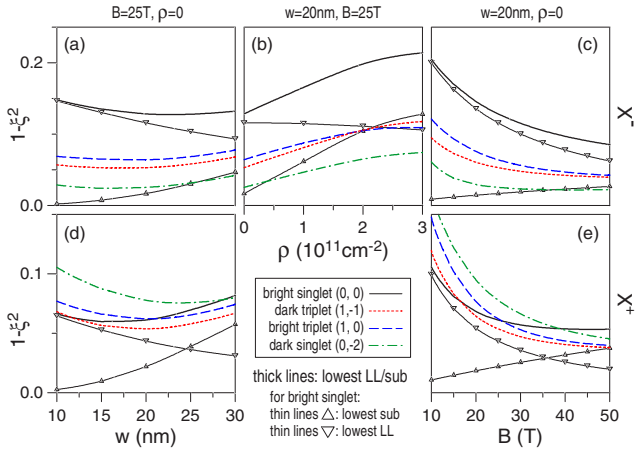

FIG. 4. (Color online) Similar to Figs. 2 and 3 but for different states of the negative (top) and positive (bottom) trions, labeled as $(S,\mathcal{M})$ by the pair electron-hole spin $S=0$ or 1 (singlet or triplet) and the relative angular momentum $\mathcal{M}$. The left, center, and right frames show dependence of $1-\xi^2$ on the well width w, electron concentration ϱ, and magnetic field B, respectively.

smaller e-h charge separation in doped wells than anticipated from the lowest-subband approximation, leading to a correspondingly weaker sensitivity of exciton PL energy or intensity to ϱ.

Figure 3 shows examples of the dependence of $1-\xi^2$ for the $k=0$ excitonic ground state on w and B. Clearly, LL mixing is stronger in narrower wells and at higher fields, while subband mixing becomes significant in the opposite limits. This results simply from the competition of Coulomb energy with the subband and cyclotron gaps, all scaling differently with w and B. As a consequence, the joint $s=n=0$ approximation appears to be of little use for the description of excitons in any realistic system.

Let us now turn to the trions. The dependences of ξ^2 on w, ϱ, and B calculated for both negative and positive states are displayed in multiple frames of Fig. 4. Different lines show $1-\xi^2_{\mathrm{LL,sub}}$ for all four bound trion states (dark and bright singlets and dark and bright triplets). Additionally, narrow black lines with triangles show $1-\xi^2_{\mathrm{sub}}$ and $1-\xi^2_{\mathrm{LL}}$ for the bright singlet state.

While the results for X, X^-, and X^+ are all qualitatively similar, the following two differences are worth noting. First, the efficiency of subband and LL mixing is quite different in different trion states, reflecting different strengths of their internal (attractive e-h and repulsive e-e or h-h) Coulomb interactions. For example, it is clear that an accurate description of the negative bright singlet trion X^-_{sb} poses the biggest problem in all realistic systems. Second, the difference between the mixing effects in X^- and X^+ is fairly weak for the triplet states, but much larger for both singlets. Note especially the big difference between the bright singlets, X^-_{sb} and X^+_{sb}, driven mostly by their very different LL mixings. The fact that the LL mixing in X^-_{sb} is much stronger than in X^+_{sb} might seem surprising when looking only at the cyclotron gaps of the e and h constituents of the X^+ and X^-. However, as we shall see further, X^-_{sb} and X^+_{sb} have quite different short-range in-plane correlations and thus also quite different internal Coulomb interactions.

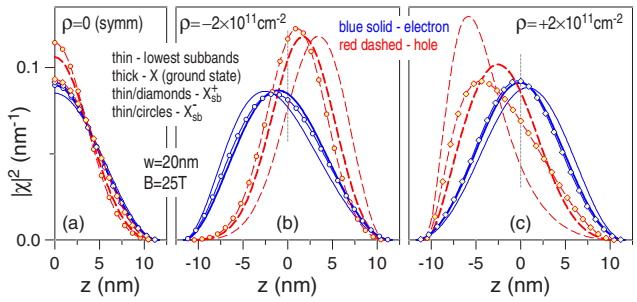

FIG. 5. (Color online) Electron and hole normal density profiles $|\chi(z)|^2$ calculated in a (a) symmetric and (b) negatively and (c) positively one-sided doped quantum-well of width $w=20$ nm, for the noninteracting carriers (the lowest single-particle subbands), the exciton (X), and the negative and positive bright singlet trions ($X^{\pm}_{\mathrm{sb}}$). The $X/X^{\pm}$ diagonalization included five Landau levels and three subbands.

C. Subband mixing

Having established the general importance of the subband mixing, let us now look in more detail at the form of exciton and trion wave functions in the growth direction, $\chi(z)$. In Fig. 5, we plot the density profiles $|\chi(z)|^2$ of an exciton ground state in three different $w=20$ nm quantum wells at $B=25$ T. In a symmetric well, the effect of subband mixing is a slight narrowing of both e and h wave functions (especially the latter), as predicted from a variational calculation in Ref. 1. In doped wells, the major effect is different and consists of the shift of e and h wave functions toward the center of the well. This can be interpreted as partial reduction of the charge separation between the noninteracting electrons and holes caused by their mutual excitonic attraction.

The average displacement of the e or h wave function from the center of the quantum well can be defined as

$$\delta = \int |\chi(z)|^2 z dz. \tag{1}$$

The standard deviation $\sigma=\sqrt{\sigma^2}$ where

$$\sigma^2 = \int |\chi(z)|^2 (z-\delta)^2 dz \tag{2}$$

can be also used to quantify the wave functions $\chi(z)$.

The plots of δ_e and δ_h as functions of k, ϱ, w, and B are shown in Fig. 6. Analogous plots of σ_e and σ_h are displayed in Fig. 7. These dependences demonstrate that the symmetric-well approximation is, in general, equally unjustified for the doped wells as the lowest-subband approximation. Moreover, knowledge of the dependence of $(\delta_e,\delta_h,\sigma_e,\sigma_h)$ on (w,ϱ,B) allows significant improvement over either of these two approximations in the calculation of the in-plane dynamics of larger excitonic complexes, such as the quasiexcitons[23] (trions coupled to the surrounding carriers). Certainly, the assumption of the excitonic normal density profiles $|\chi_e(z)|^2$ and $|\chi_h(z)|^2$ for larger complexes would ignore both normal correlations and the possible dependence of $\chi(z)$ on the studied complex itself. In other words, it would rely on the strong spatial quantization in the normal

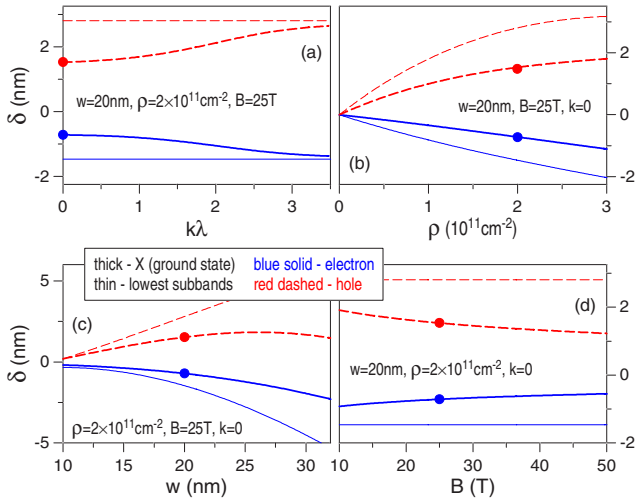

FIG. 6. (Color online) The average displacements δ of the electron and hole normal density profiles $|\chi(z)|^2$ from the center of the quantum well, calculated for both the noninteracting carriers and (including five Landau levels and three subbands in the diagonalization) for the exciton (X) and drawn as a function of the (a) excitonic wave vector k (λ is the magnetic length), (b) electron concentration ϱ, (c) well width w, and (d) magnetic field B. The dots mark the same state in each frame ($w=20$ nm, $\varrho=2\times10^{11}$ cm^{-2}, $B=25$ T, and $k=0$).

direction and on the decoupling of the normal and in-plane dynamics (adiabatic approximation). However, a more exact treatment of subband mixing is virtually impossible for the quasiexcitons for their too complicated in-plane dynamics. Nevertheless, this approach will here remain unexploited as we focus on the (relatively simpler) excitons and trions.

Our discussion of trions begins with Fig. 8, which compares δ and σ of the lowest subbands, the exciton ground state, and different negative trions for the same parameters as used in Fig. 5. For the symmetric well, the present exact-diagonalization calculation essentially confirms the qualitative results of the (less reliable) variational approach of Ref. 1. Specifically, (i) the interaction-induced narrowing of $\chi(z)$ is much stronger for the hole than for the electrons, which further enhances the $\sigma_h<\sigma_e$ asymmetry; (ii) σ_h varies appreciably between different exciton and trion states; and (iii) σ_h is smaller in the trions than in the exciton, while σ_e does the opposite.

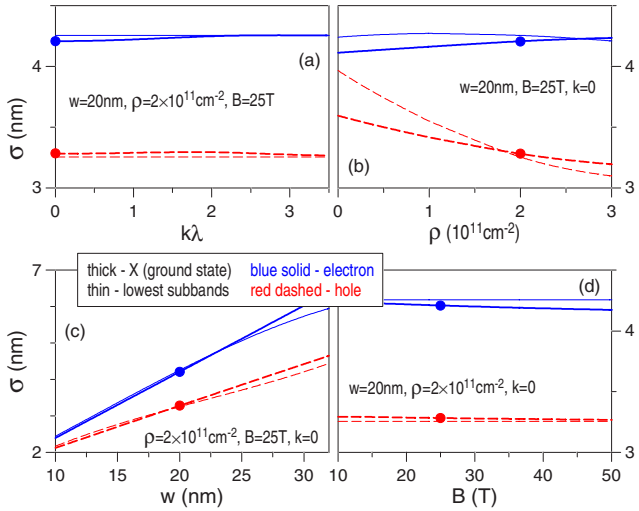

FIG. 7. (Color online) Same as Fig. 6 but for the standard deviations σ of the profiles $|\chi(z)|^2$ from the average values δ.

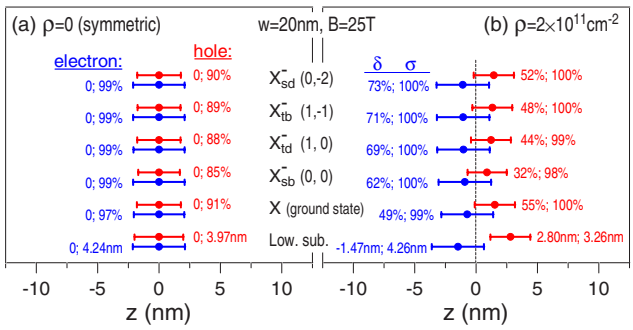

FIG. 8. (Color online) Comparison of average displacements δ and their standard deviations σ calculated from the electron and hole normal density profiles $|\chi(z)|^2$ of the noninteracting carriers (lowest subbands), the exciton (X), and different negative trions (X^-) labeled by $(S,\mathcal{M})$ as in Fig. 4, in the (a) symmetric and (b) one-sided doped quantum wells. For X and X^-, the labels δ, σ are given relative to the values for the lowest subbands (which are expressed in nanometers).

Let us add a few values for the positive trions in the same well, not shown in Fig. 8(a). Relative to the lowest-subband values, we find $(\sigma_e,\sigma_h)=(96\%,99\%)$ for X^+_{sb} and (96%, 96%) for X^+_{td}, X^+_{tb}, and X^+_{sd}.

The asymmetric wells are less susceptible to the variational calculation and thus were not studied in Ref. 1. Here, in the n-doped well, we find that σ_e and σ_h are both virtually insensitive to the exciton or trion binding, and the main subband-mixing effect involves δ_e and δ_h. In particular, we find that δ_h is slightly smaller in the trions than in the exciton, but δ_e clearly does the opposite.

Let us also list the corresponding numbers for the positive trions in an asymmetric $w=20$ nm well with the hole concentration $\varrho=2\times10^{11}$ cm^{-2}. Here (in the units of nanometers), we find $(\delta_e,\delta_h)=(-0.22,-2.22)$, $(-0.27,-2.59)$, $(-0.12,-2.85)$, and $(-0.22,-2.82)$ for X^+_{sb}, X^+_{td}, X^+_{tb}, and X^+_{sd}, respectively, compared to $(-0.06,-1.96)$ for the X or $(0.52,-4.13)$ for the lowest subbands. Note that the e-h attraction in the X/X^+ states is sufficient to change the sign of δ_e [i.e., to pull the electron toward the hole(s) across the center of the quantum well]. Let us also list for this p-doped well the following: $(\sigma_e,\sigma+h)=(97\%,121\%)$, (97%, 114%), (98%, 112%), and (98%, 111%) for X^+_{sb}, X^+_{td}, X^+_{tb}, and X^+_{sd}, respectively, and (98%, 109%). Note that while δ_e remains nearly unaffected by the e-h attraction, δ_h is considerably increased (in contrast to the n-doped well), weakening the $\delta_e<\delta_h$ asymmetry of the lowest subbands.

In Fig. 9, we compare the average e-h displacements $\delta_{eh}=|\delta_e-\delta_h|$ in the exciton ground state and in different negative trions on the example of three dependences on w, ϱ, and B. The significant reduction of δ_{eh} compared to the lowest subbands is again evident in all states and for all shown

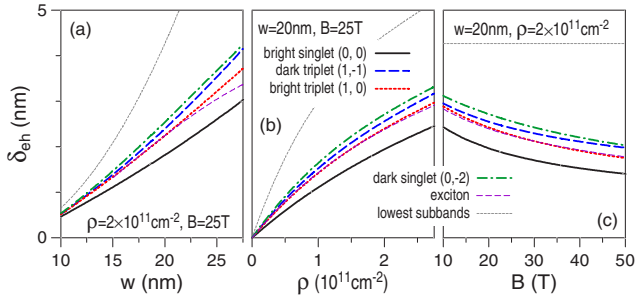

FIG. 9. (Color online) Average electron-hole normal displacement $\delta_{eh}=|\delta_e-\delta_h|$ calculated for both the noninteracting carriers and (including five Landau levels and three subbands) for the exciton (X) and different negative trions (X^-) labeled by $(S,\mathcal{M})$ as in Fig. 4, drawn as a function of (a) well width w, (b) electron concentration ϱ, and (c) magnetic field B.

parameters. The largest reduction generally occurs for $X^-_{\rm sb}$, while the exciton and other trions have slightly larger values of δ_{eh} (note also the similarity of X and $X^-_{\rm tb}$). This occurs regardless of the ordering of trion binding energies, depending more on the e-h attraction and e-e repulsion being (separately) the strongest in $X^-_{\rm sb}$.

D. In-plane correlation functions

In contrast to the strongly quantized motion in the z direction, rather well characterized by the separate e and h density profiles $|\chi(z)|^2$, the free in-plane motion needs to be described in terms of mutual correlations. Several examples of the in-plane e-h pair-correlation function $g_{eh}(r)$ of the exciton have been shown in Fig. 10. Here, r is the 2D separation, and g is normalized to $\lambda^{-2}\int g(r)rdr=1$, where λ is the magnetic length. In frame (a), we plot $g_{eh}(r)$ for several different wave vectors k marked on the exciton energy dispersion in the inset (c). These values of k correspond to the indicated total angular momenta $L=kR$ (with $R=\sqrt{10}\lambda$ being the radius of the Haldane sphere used in the calculation). It is evident that the exciton's motion causes e-h charge separation (the resulting perpendicular electric dipole moment will be discussed in a later section). In frame (b), we compare $g_{eh}(r)$ for the $k=0$ ground state in several systems defined by (w,ϱ,B). Not surprisingly, $g_{eh}(r)$ depends more strongly on the magnetic field (through the predominantly B-dependent LL mixing) than on the well parameters, even for r expressed in the magnetic units.

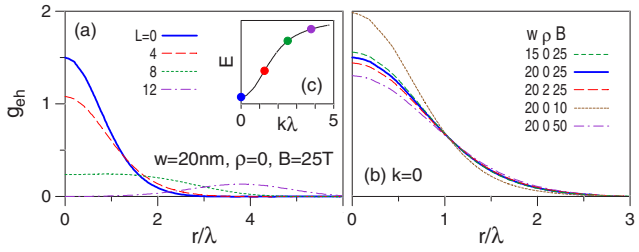

FIG. 10. (Color online) Comparison of electron-hole pair-correlation functions $g_{eh}(r)$ of the exciton with (a) different wave vectors k (the chosen values of k are marked on the excitonic energy dispersion shown in the inset (c) and correspond to the indicated angular momenta L on a sphere with magnetic monopole strength $2Q=20$; λ is the magnetic length) and (b) with the $k=0$ excitonic ground state in quantum wells with different widths w (given in nm), electron concentrations ϱ (in 10^{11} cm^{-2}), and different magnetic fields B (in T).

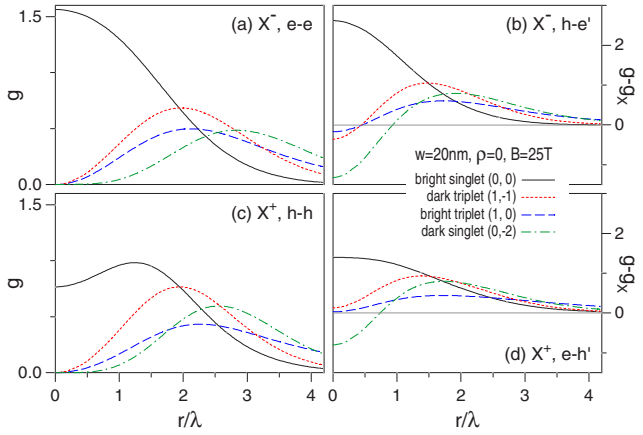

FIG. 11. (Color online) (a) Electron-electron, (b) hole–second-electron, (c) hole-hole, and (d) electron–second-hole pair-correlation functions [denoted as $g_{ee}(r)$, $g_{he'}(r)$, $g_{hh}(r)$, and $g_{eh'}(r)$, respectively] of different states of the negative and positive trions ($X^{\pm}$) labeled by $(S,\mathcal{M})$ as in Fig. 4, calculated in a symmetric $w=20$ nm quantum well at the magnetic field $B=25$ T. λ is the magnetic length.

The correlation functions of negative and positive trions in a symmetric $w=20$ nm well at $B=25$ T have been shown in Fig. 11. For the X^-, in addition to g_{ee}, instead of $g_{eh}\equiv g_{eh}[X^-]$, we also plot $g_{he'}=2g_{eh}[X^-]-g_{eh}[X]$, which can be interpreted as describing the correlation between the single hole (h) and the second electron (e'). Analogously, for the X^+, we plot $g_{eh'}=2g_{eh}[X^+]-g_{eh}[X]$. Clearly, the similarity between the corresponding X^- and X^+ states is much greater than that between different X^- states or between different X^+ states. However, there is one remarkable exception:[34] the short-range e-e and h-h correlations in the negative and positive bright singlet trions are quite different.

The $X^-_{\rm sb}/X^+_{\rm sb}$ asymmetry is illustrated more clearly in Fig. 12, where we magnify and compare directly the short-range parts of g_{ee} and g_{hh} of the bright singlet states of the negative and positive trions in several different systems. Obviously, the X^-/X^+ asymmetry is due to the difference between electron and hole effective masses, but it is remarkable that it is so much stronger in the bright singlet states than in the other trions. It is also noteworthy in Fig. 12 that the wave function of $X^+_{\rm sb}$ is much more sensitive to w and B than that of $X^-_{\rm sb}$.

In Fig. 13, we plot the average in-plane separations

$$d=\lambda^{-2}\int g(r)r^2dr. \tag{3}$$

Different frames show examples of dependences of the excitonic d_{eh} as well as of d_{ee} and $d_{he'}$ of the different negative trions on w, ϱ, or B. They demonstrate (i) significant differ-

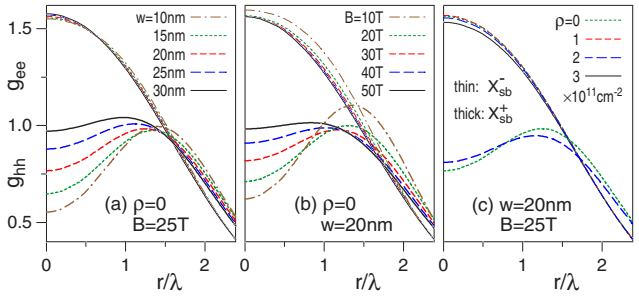

FIG. 12. (Color online) Comparison of the short-range parts of electron-electron (g_{ee}) and hole-hole (g_{hh}) pair-correlation functions of the negative and positive bright singlet trions (X^-_{sb} and X^+_{sb}) in quantum wells of (a) different widths w, (b) magnetic fields B, and (c) electron and/or hole concentrations. ϱ. λ is the magnetic length.

ence between the correlation parameters d in different trion states and (ii) stability of correlations parameters under variation of well parameters (e.g., $d_{eh}/\lambda \approx 1$, 1.5, 2, 3, and 3 for X, X^-_{sb}, X^-_{td}, X^-_{tb}, and X^-_{sd}, respectively), especially for the X, X^-_{sb}, and X^-_{td}.

Similar plots of d_{hh} and $d_{eh'}$ as a function of w and B for the positive trions have been shown in Figs. 14(a) and 14(b), and $d_{eh'}(w)$ for X^+ and $d_{he'}(w)$ for X^- have been drawn together in Fig. 14(c). The latter graph contrasts the difference between X^+_{sb} and X^-_{sb} with the similarity of X^+_{td} and X^-_{td}. This contrast is consistent with the significant asymmetry in the $X^\pm_{sb}$ binding energies well known from the earlier experiment[25] and numerics[34] and the near symmetry of $\Delta^\pm_{td}$ and $\Delta^\pm_{tb}$ (see e.g., Table I).

As another, arguably more convincing way to compare X^+ and X^-, in Fig. 15, we have shown their squared overlaps $|\langle X^-|\mathcal{T}_{eh}|X^+\rangle|^2$, where $\mathcal{T}_{eh}$ denotes the $e \leftrightarrow h$ charge conjugation. To emphasize the comparison of in-plane correlations, with thin lines, we have also plotted the overlaps calculated after the projection of $|X^\pm\rangle$ onto the lowest subbands, followed by renormalization ($X^\pm$ eigenstates $\rightarrow$ projection $\rightarrow$ normalization $\rightarrow$ overlap). Consistently with the correlation analysis, the X^+_{sb}/X^-_{sb} overlap is the lowest ($<90\%$) for nearly all parameters and the X^+_{td}/X^-_{td} overlap is usually the largest ($>95\%$).

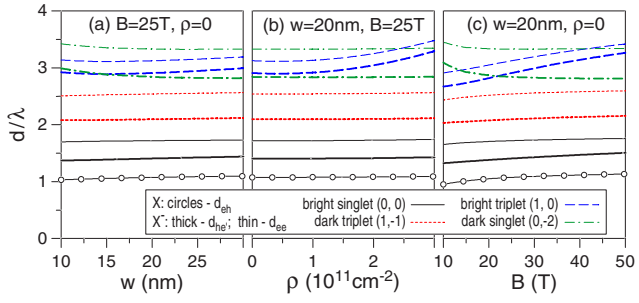

FIG. 13. (Color online) Average in-plane electron-electron, electron-hole, and hole–second-electron separations (denoted by d_{ee}, d_{eh}, and $d_{he'}$, respectively) of the exciton (X) and different states of the negative trion (X^-) labeled by $(S,\mathcal{M})$ as in Fig. 4, drawn as a function of the (a) well width w, (b) electron concentration ϱ, and (c) magnetic field B. λ is the magnetic length.

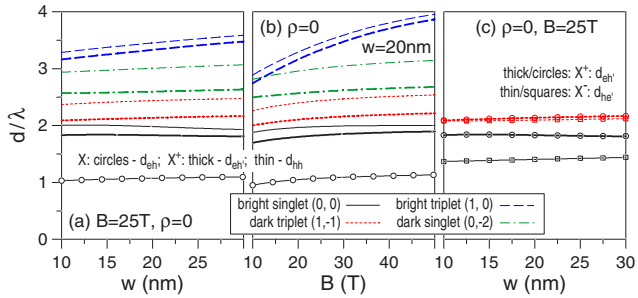

FIG. 14. (Color online) [(a) and (b)] Same as Fig. 13 but for positive trions (X^+). (c) Comparison between $d_{eh'}$ of the bright singlet and dark triplet states of the X^+ and $d_{he'}$ of the corresponding states of the X^-.

Since pair states of identical charges in a magnetic field are distinguished by a quantized angular momentum (in contrast to pair states of opposite charges labeled by a continuous wave vector), certain features of the relative e-e or h-h motion in the trions can be identified more easily from the discrete version of the corresponding pair-correlation functions. In Fig. 16, we compare Haldane amplitudes $\mathcal{G}(\mathcal{R})$ of the negative and positive trions in a symmetric $w=20$ nm well at $B=25$ T. The amplitudes $\mathcal{G}_{ee}$ and $\mathcal{G}_{hh}$ are defined as the occupation of e-e or h-h pair states with the relative angular momentum $\mathcal{R}$, normalized to $\Sigma_{\mathcal{R}}\mathcal{G}(\mathcal{R})=1$. Within the lowest LL (containing nearly the entire trion wave functions in this example), $\mathcal{R}$ must be even and odd for the spin singlet and triplet states, respectively, so only those allowed parameters have been shown.

Clearly, the e-e correlations in X^-_{sb} and X^-_{td} (or the h-h correlations in X^+_{sb} and X^+_{td}) can be captured very simply as $\mathcal{R}_{sb} \approx 0$ and $\mathcal{R}_{td} \approx 1$, respectively. For the other trions, especially for $X^\pm_{tb}$, mixing of different e-e or h-h pair states is more efficient. For $X^\pm_{sd}$, it appears that $\mathcal{R}_{sd} \geqslant 2$. The X^-/X^+ asymmetry can also be observed, but it does not appear significant.

E. Oscillator strengths

The exciton and trion oscillator strengths I_{if} for the $i \rightarrow f$ optical recombination have been calculated from the Fermi golden rule,

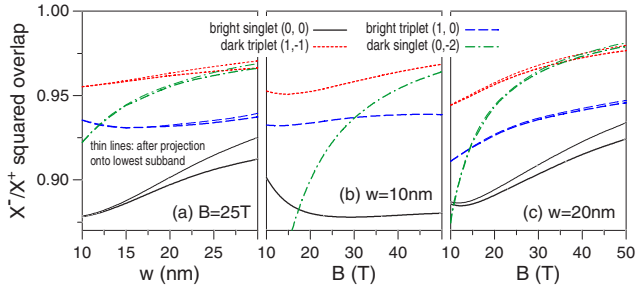

FIG. 15. (Color online) Squared overlaps of the corresponding negative and positive trion states (X^- and X^+) labeled by $(S,\mathcal{M})$ as in Fig. 4, drawn as a function of the (a) well width w and [(b) and (c)] magnetic field B. Thin lines give the squared overlaps between the renormalized projections of the compared X^- and X^+ states onto the lowest subbands (thereby isolating the in-plane dynamics).

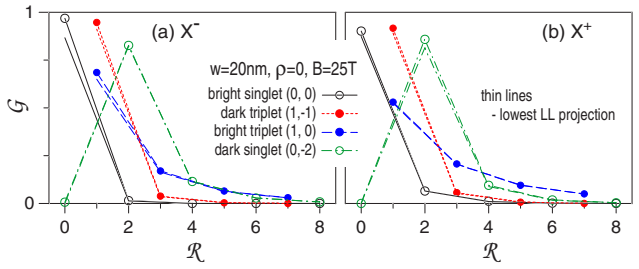

FIG. 16. (Color online) Discrete electron-electron and hole-hole pair-correlation functions (Haldane pair amplitudes $\mathcal{G}$ as a function of the relative pair angular momentum $\mathcal{R}$) of the (a) negative and (b) positive trions labeled by $(S,\mathcal{M})$ as in Fig. 4. Thin lines give $\mathcal{G}(\mathcal{R})$ for the projection of the trion wave functions onto the lowest Landau level.

$$I_{if} = |\langle f|\mathcal{I}_{eh}|i\rangle|^2, \tag{4}$$

where $i=X$ or $X^{\pm}$, $f=$vac, e, or h, and $\mathcal{I}_{eh}$ is the optical e-h annihilation operator.

The optical spectrum of an exciton involves different $k=0$ states, each opening a continuous band derived from the noninteracting bands with different optically active combinations of n_e, n_h, s_e, and s_h (i.e., $n_e=n_h$ because of the 2D magnetic translational symmetry[33] and, in symmetric wells, $s_e=s_h$ due to parity conservation). All these transitions, shown in the left frames of Fig. 17, can, in principle, be observed in absorption. However, in low-temperature PL, only the lowest initial active state is of interest, corresponding to $I_{if}\equiv I^0$.

For the free trions, the pair of dark states is optically inactive, and the recombination spectra of $X^{\pm}_{\rm sb}$ and $X^{\pm}_{\rm tb}$ are dominated by the transitions to the electron or hole in the lowest subband and lowest LL. The shake-up processes involving excitation to a higher LL of the carrier left over in the finite state are forbidden[35,36] by the conservation of angular momenta (L and L_z on a sphere or $\mathcal{M}$ and M on a plane). On the other hand, the intersubband shake-up is allowed, with the parity-conservation selection rule relaxed by the asymmetry of doped wells. However, as shown in the right frames of Fig. 17, the intersubband shake-up processes remain at least 3 orders of magnitude weaker than the main recombination channel for the doped $w=20$ nm well we chose as the example. Excluding shake-up, for the main recombination channels, we can define $I_{if}\equiv I^-_{\rm sb}$, $I^-_{\rm tb}$, $I^+_{\rm sb}$, and $I^+_{\rm tb}$, all compared with the excitonic I^0 in Fig. 18, showing the examples of dependence on w, ϱ, and B. This figure can be summarized as follows: (i) the dependences of I on w (increasing) and on ϱ and B (decreasing) are all stronger for the exciton than for the trions, and (ii) $I^0>I^{\pm}_{\rm tb}>I^{\pm}_{\rm sb}$ and $I^+>I^-$ for all studied parameters.

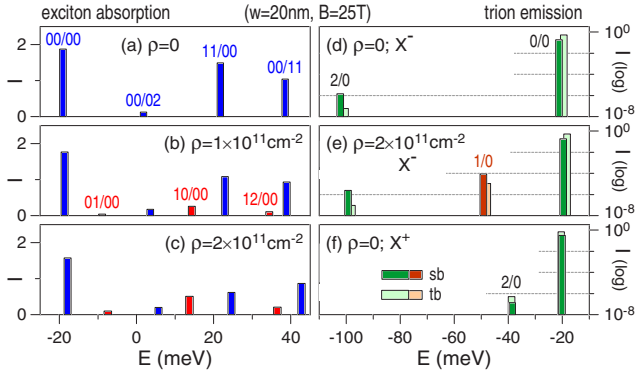

FIG. 17. (Color online) Left: Exciton absorption spectrum (dependence of oscillator strength I on transition energy E counted from a noninteracting electron-hole pair). Labels s_es_h/n_en_h indicate subband and Landau level quantum numbers of a photocreated pair. Transitions shown with red bars violate s parity and are only allowed in asymmetric wells. Right: Recombination spectra of negative (X^-) and positive (X^+) bright trions. Labels s/n indicate quantum numbers of the single carrier left over in the final state. Transitions with $s>0$ represent the weak (note a logarithmic I scale) intersubband shake-up. Red bars mark odd-s transitions, forbidden in symmetric wells by the s-parity conservation.

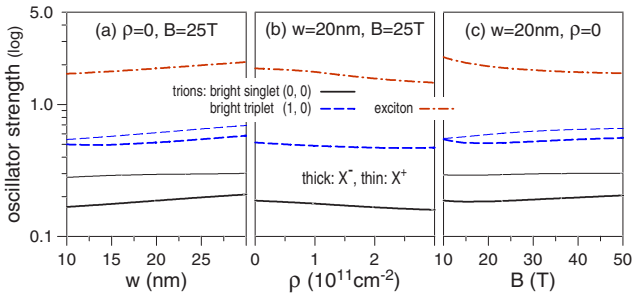

FIG. 18. (Color online) Oscillator strengths I^0 and $I^{\pm}$ of the main exciton (X) and bright trion ($X^{\pm}$) recombination channels, drawn as a function of the (a) well width w, (b) electron concentration ϱ, and (c) magnetic field B.

F. Exciton dipole moment

The last characteristic we have analyzed is the transverse electric dipole moment $e\tau$, acquired by the exciton moving in a magnetic field. In order to calculate τ (the average e-h separation in the direction normal to both magnetic field and wave vector), we have determined the lowest-energy exciton eigenstates at different values of $L=L_z$. These states represent the motion of the exciton along the equator, with the wave vector given by $k\lambda=L/R$ (where R is the sphere radius). In these states, τ can be easily calculated from the average electron and hole values of $Z=R\cos\theta$ (where θ is the standard spherical coordinate). The matrix elements of $\cos\theta$ are[37]

$$\langle n,m|\cos\theta|n,m\rangle = \frac{Qm}{l(l+1)}, \tag{5}$$

$$\langle n-1,m|\cos\theta|n,m\rangle = \sqrt{\frac{(l^2-m^2)(l^2-Q^2)}{l^2(4l^2-1)}}. \tag{6}$$

The averages $\langle Z_e\rangle$ and $\langle Z_h\rangle$ calculated in the particular excitonic eigenstates were then converted into the average displacements τ_e and τ_h measured from the equator along the

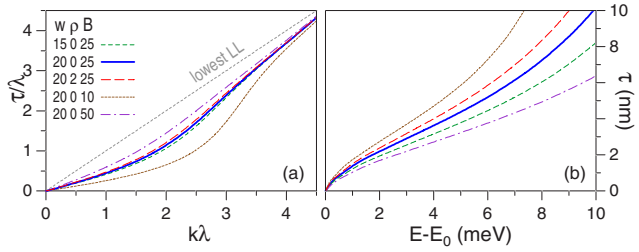

FIG. 19. (Color online) Average electron-hole transverse separation τ (proportional to the electric dipole moment $e\tau$) of an exciton, drawn as a function of (a) wave vector k or (b) the excitation energy $E-E_0$ (E_0 being the energy of the $k=0$ ground state) in quantum wells with different widths w (given in nm) and electron concentrations ϱ (in 10^{11} cm^{-2}) and in different magnetic fields B (in T). λ is the magnetic length.

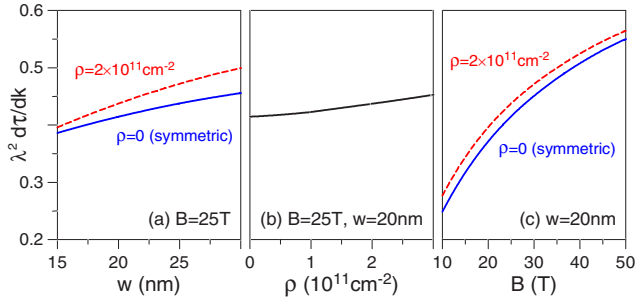

FIG. 20. (Color online) Slope of the exciton's $\tau(k)$ at $k=0$ (calculated from the curves like those in Fig. 19 in order to compare with $\lambda^2 d\tau/dk=1$ in the lowest Landau level), drawn as a function of the (a) well width w, (b) electron concentration ϱ, and (c) magnetic field B.

surface of the sphere, e.g., $\langle Z_e\rangle=\cos(\pi/2-\tau_e/R)$. Finally, the transverse e-h separation was defined as $\tau=|\tau_e-\tau_h|$.

As a reference for τ, we choose the value for an exciton in the lowest LL. For the $L=L_z$ state of an e-h pair in the lowest LL on a sphere with the magnetic monopole strength $2Q$, we find $\langle Z\rangle=\pm L/(2Q+2)$ which, in the limit of $\lambda/R\to 0$, yields a known result, $\tau=k\lambda^2$.

In Fig. 19(a), we show that the LL mixing decreases $\tau\lambda^{-1}$ at a given $k\lambda$. Thus, the dimensionless function $\tau\lambda^{-1}(k\lambda)$ depends rather strongly on B and much less on w or ϱ. The conversion of this function into the dependence of the dipole moment on the excitation energy is shown in Fig. 19(b). This graph compares the energy cost needed to produce the dipole moment of a given magnitude by an exciton. Since this dipole moment is responsible for the exciton-electron interaction and the trion binding, Fig. 19(b) conforms to the general (though not absolutely universal) tendency that the trion binding is enhanced by large B and by small w and ϱ.

The crucial feature of the dependence $\tau(k)$ is the reduction of the slope at small wave vectors compared to $d\tau/dk=\lambda^{-2}$ of the lowest LL. This slope is plotted as a function of w, ϱ, and B in Fig. 20 to confirm that, generally, $d\tau/dk<\lambda^{-2}$ and that the sensitivity to the magnetic field is stronger than to the quantum-well parameters (within the considered ranges).

IV. CONCLUSION

Using exact numerical diagonalization on a Haldane sphere, we have calculated the wave functions of free excitons (X) and trions ($X^{\pm}$) confined in the GaAs quantum wells of width $w=10-30$ nm, doped on one side to the electron or hole concentration $\varrho=0$ to 2×10^{11} cm^{-2}, and subject to the magnetic field $B=10-50$ T. From these wave functions, we have obtained and analyzed the efficiency of subband and Landau level mixing $1-\xi^2$, the displacement δ and width σ of electron and hole normal charge density profiles $|\chi(z)|^2$, the continuous and discrete in-plane pair-correlation functions $g(r)$ and $\mathcal{G}(\mathcal{R})$, the oscillator strengths I for radiative absorption or recombination, and also (for the moving excitons) the transverse electric dipole moment $e\tau$. These characteristics of the exciton and trion states were studied as a function of w, ϱ, B, and the excitonic wave vector k.

We have also carried out a detailed comparison of the corresponding states of the negative and positive trions. The main qualitative difference is between the short-range electron-electron and hole-hole correlations in the bright singlet states, $X^-_{\rm sb}$ and $X^+_{\rm sb}$. Remarkably, this asymmetry (obviously caused by a larger effective mass of the hole) much less affects the other bound trion states (e.g., the pair of triplets). It explains several differences between $X^-_{\rm sb}$ and $X^+_{\rm sb}$, including the significantly weaker (by a factor of about two) binding of the positive state, known earlier from the PL spectra.

Further research could be directed toward interaction of the excitonic complexes with surface fluctuations[38] or (nearby or remote) ionized impurities.[36] The motivation for such calculation is that this interaction could easily be responsible for the slight but noticeable disparity between the trion binding energies Δ calculated assuming perfect translational invariance and those extracted from the PL measurements. Especially, the critical magnetic field for the singlet-triplet transition in the trion ground state appears to be consistently and significantly overestimated in the free trion calculations. However, these results will be postponed for a separate publication.

ACKNOWLEDGMENTS

The author thanks Leszek Bryja and John J. Quinn for helpful discussions and acknowledge partial support from Grant No. N202-071-32/1513 of the Polish MNiSW.

[1] A. Wójs and J. J. Quinn, Phys. Rev. B **75**, 085318 (2007).
[2] M. A. Lampert, Phys. Rev. Lett. **1**, 450 (1958).
[3] K. Kheng, R. T. Cox, Y. Merle d'Aubigne, F. Bassani, K. Saminadayar, and S. Tatarenko, Phys. Rev. Lett. **71**, 1752 (1993).
[4] For exhaustive reviews, see F. M. Peeters, C. Riva, and K. Varga, Physica B **300**, 139 (2001); I. Bar-Joseph, Semicond. Sci. Technol. **20**, R29 (2005). A more extensive introduction was also included in Ref. 1 preceding this paper.
[5] B. Stebe and A. Ainane, Superlattices Microstruct. **5**, 545 (1989).
[6] H. Buhmann, L. Mansouri, J. Wang, P. H. Beton, N. Mori, L. Eaves, M. Henini, and M. Potemski, Phys. Rev. B **51**, 7969 (1995).
[7] G. Finkelstein, H. Shtrikman, and I. Bar-Joseph, Phys. Rev. Lett. **74**, 976 (1995); Phys. Rev. B **53**, R1709 (1996).
[8] A. J. Shields, M. Pepper, M. Y. Simmons, and D. A. Ritchie, Phys. Rev. B **52**, 7841 (1995).
[9] A. Wójs and P. Hawrylak, Phys. Rev. B **51**, 10880 (1995).
[10] J. J. Palacios, D. Yoshioka, and A. H. MacDonald, Phys. Rev. B **54**, R2296 (1996).
[11] A. Wójs, J. J. Quinn, and P. Hawrylak, Phys. Rev. B **62**, 4630 (2000).
[12] G. Yusa, H. Shtrikman, and I. Bar-Joseph, Phys. Rev. Lett. **87**, 216402 (2001).
[13] D. M. Whittaker and A. J. Shields, Phys. Rev. B **56**, 15185 (1997).
[14] C. Riva, F. M. Peeters, and K. Varga, Phys. Rev. B **61**, 13873 (2000); **63**, 115302 (2001).
[15] P. Redlinski and J. Kossut, Solid State Commun. **118**, 295 (2001); Semicond. Sci. Technol. **17**, 237 (2002); P. Redlinski, J. Appl. Phys. **99**, 063702 (2006).
[16] A. J. Shields, J. L. Osborne, M. Y. Simmons, M. Pepper, and D. A. Ritchie, Phys. Rev. B **52**, R5523 (1995).
[17] D. Gekhtman, E. Cohen, A. Ron, and L. N. Pfeiffer, Phys. Rev. B **54**, 10320 (1996).
[18] G. V. Astakhov, D. R. Yakovlev, V. P. Kochereshko, W. Ossau, J. Nürnberger, W. Faschinger, and G. Landwehr, Phys. Rev. B **60**, R8485 (1999); G. V. Astakhov, D. R. Yakovlev, V. P. Kochereshko, W. Ossau, W. Faschinger, J. Puls, F. Henneberger, S. A. Crooker, Q. McCulloch, D. Wolverson, N. A. Gippius, and A. Waag, *ibid.* **65**, 165335 (2002).
[19] T. Vanhoucke, M. Hayne, V. V. Moshchalkov, and M. Henini, Nanotechnology **11**, 281 (2000); T. Vanhoucke, M. Hayne, M. Henini, and V. V. Moshchalkov, Phys. Rev. B **63**, 125331 (2001); **65**, 041307 (2002); **65**, 233305 (2002).
[20] C. Schüller, K.-B. Broocks, Ch. Heyn, and D. Heitmann, Phys. Rev. B **65**, 081301(R) (2002); C. Schuller, K. B. Broocks, P. Schroter, C. Heyn, D. Heitmann, M. Bichler, W. Wegscheider, T. Chakraborty, and V. M. Apalkov, Phys. Rev. Lett. **91**, 116403 (2003).
[21] J. G. Groshaus, P. Plochocka-Polack, M. Rappaport, V. Umansky, I. Bar-Joseph, B. S. Dennis, L. N. Pfeiffer, K. W. West, Y. Gallais, and A. Pinczuk, Phys. Rev. Lett. **98**, 156803 (2007).
[22] A. Wójs, P. Hawrylak, and J. J. Quinn, Phys. Rev. B **60**, 11661 (1999); A. Wójs, I. Szlufarska, K.-S. Yi, and J. J. Quinn, *ibid.* **60**, R11273 (1999).
[23] A. Wójs, A. Gładysiewicz, and J. J. Quinn, Phys. Rev. B **73**, 235338 (2006).
[24] M. Byszewski, B. Chwalisz, D. K. Maude, M. L. Sadowski, M. Potemski, T. Saku, Y. Hirayama, S. Studenikin, D. G. Austing, A. S. Sachrajda, and P. Hawrylak, Nat. Phys. **2**, 239 (2006).
[25] S. Glasberg, G. Finkelstein, H. Shtrikman, and I. Bar-Joseph, Phys. Rev. B **59**, R10425 (1999).
[26] F. D. M. Haldane, Phys. Rev. Lett. **51**, 605 (1983).
[27] M. Rontani, C. Cavazzoni, D. Bellucci, and G. Goldoni, J. Chem. Phys. **124**, 124102 (2006).
[28] M. J. Snelling, G. P. Flinn, A. S. Plaut, R. T. Harley, A. C. Tropper, R. Eccleston, and C. C. Phillips, Phys. Rev. B **44**, 11345 (1991).
[29] M. Hayne, C. L. Jones, R. Bogaerts, C. Riva, A. Usher, F. M. Peeters, F. Herlach, V. V. Moshchalkov, and M. Henini, Phys. Rev. B **59**, 2927 (1999).
[30] G. V. Astakhov, D. R. Yakovlev, V. V. Rudenkov, P. C. M. Christianen, T. Barrick, S. A. Crooker, A. B. Dzyubenko, W. Ossau, J. C. Maan, G. Karczewski, and T. Wojtowicz Phys. Rev. B **71**, 201312(R) (2005).
[31] D. Andronikov, V. Kochereshko, A. Platonov, T. Barrick, S. A. Crooker, and G. Karczewski Phys. Rev. B **72**, 165339 (2005).
[32] A. B. Dzyubenko and Yu. E. Lozovik, Fiz. Tverd. Tela (Leningrad) **25**, 1519 (1983) [Sov. Phys. Solid State **25**, 874 (1983)].
[33] A. B. Dzyubenko and A. Y. Sivachenko, Phys. Rev. Lett. **84**, 4429 (2000); A. B. Dzyubenko, Solid State Commun. **113**, 683 (2000).
[34] C. Riva, F. M. Peeters, and K. Varga, Phys. Rev. B **64**, 235301 (2001).
[35] A. B. Dzyubenko, Phys. Rev. B **69**, 115332 (2004).
[36] L. Bryja, A. Wójs, J. Misiewicz, M. Potemski, D. Reuter, and A. Wieck, Phys. Rev. B **75**, 035308 (2007).
[37] A. Wójs and J. J. Quinn, Physica E (Amsterdam) **3**, 181 (1998).
[38] A. V. Filinov, C. Riva, F. M. Peeters, Yu. E. Lozovik, and M. Bonitz, Phys. Rev. B **70**, 035323 (2004).